International Journal of Extreme Manufacturing

Molecular dynamics simulation of the material removal in the scratching of 4H-SiC and 6H-SiC substrates

To cite this article: Zige Tian *et al* 2020 *Int. J. Extrem. Manuf.* **2** 045104

OPEN ACCESS
IOP Publishing | IMMT
International Journal of Extreme Manufacturing
Int. J. Extrem. Manuf. **2** (2020) 045104 (15pp)
https://doi.org/10.1088/2631-7990/abc26c

Molecular dynamics simulation of the material removal in the scratching of 4H-SiC and 6H-SiC substrates

Zige Tian[1,2], **Xun Chen**[2] and **Xipeng Xu**[1]

[1] Institute of Manufacturing Engineering, Huaqiao University, Xiamen, Fujian Province, People's Republic of China
[2] Faculty of Engineering and Technology, Liverpool John Moores University, Liverpool, United Kingdom

E-mail: x.chen@ljmu.ac.uk

Received 28 May 2020, revised 14 July 2020
Accepted for publication 19 October 2020
Published 4 November 2020

Abstract

Single crystal silicon carbide (SiC) is widely used for optoelectronics applications. Due to the anisotropic characteristics of single crystal materials, the C face and Si face of single crystal SiC have different physical properties, which may fit for particular application purposes. This paper presents an investigation of the material removal and associated subsurface defects in a set of scratching tests on the C face and Si face of 4H-SiC and 6H-SiC materials using molecular dynamics simulations. The investigation reveals that the sample material deformation consists of plastic, amorphous transformations and dislocation slips that may be prone to brittle split. The results showed that the material removal at the C face is more effective with less amorphous deformation than that at the Si face. Such a phenomenon in scratching relates to the dislocations on the basal plane (0001) of the SiC crystal. Subsurface defects were reduced by applying scratching cut depths equal to integer multiples of a half molecular lattice thickness, which formed a foundation for selecting machining control parameters for the best surface quality.

Keywords: material removal mechanism, molecular dynamics simulation, subsurface defects, scratching, 4H-SiC and 6H-SiC

(Some figures may appear in colour only in the online journal)

1. Introduction

Single crystal silicon carbide (SiC) has extensive applications in microelectronics, optoelectronics, aerospace, and medical sectors because of its specific properties, such as chemical inertness, high thermal conductivity, high specific stiffness, and high-temperature stability [1]. In more than 250 polytypes of SiC, 4H-SiC has wide applications for optoelectronic devices, high-temperature electronic devices, ultra-precision micro/nano dies, and high-performance mirrors; and 6H-SiC is primarily used in optoelectronic devices, such as laser diodes and blue light emitting diodes [2–5]. These ultra-precision components require atomically smooth and damage-free surfaces, any defects, even at the nanoscale, derived from the growth of SiC or its machining process threaten SiC-based device performance [6].

In order to eliminate defects from SiC surfaces and improve polishing efficiency, a better understanding of material removal mechanisms at the molecular level is critical. Considering the SiC crystal structure, it is inevitable and necessary to identify and evaluate different machining mechanisms and effectiveness for the crystal faces of SiC. Therefore, investigations of the nanoscale mechanical properties and machining mechanisms of 4H-SiC and 6H-SiC substrates have attracted significant attention in recent years. Indentation

2631-7990/20/045104+15$33.00

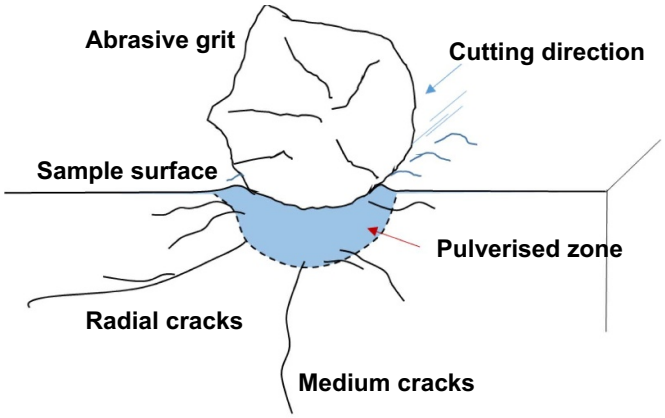

Figure 1. Subsurface damage of brittle materials in micron-scale cutting.

and scratching experiments on 4H-SiC and 6H-SiC are two common methods of studying the nanomechanical properties of materials. Indentation load-displacement curves show that yielding or incipient plasticity in 4H-SiC and 6H-SiC happens at shear stresses of 21 GPa and 23.4 GPa with a pop-in event [7, 8]. Consequential material deformation and failure behaviour and the transitional conditions between elastic, plastic, and fracture were observed and analysed with these methods. Grim *et al* [9] experimentally confirmed that basal dislocation can also be activated in the subsurface of 6H-SiC during mechanical polishing. Meng *et al* [10] undertook a series of nano-scratching tests to investigate subsurface structures before and after scratching. By observing the results from transmission electron microscopy (TEM), they found some micro-cracks on the subsurface with lengths (up to 1 μm) many times longer than the processed depth (90 nm). The subsurface damage may relate to lattice mismatch and bond rupture. Dislocations can also lead to cracks. Zhang *et al* [11] observed diamond scratching on alumina samples. Their results showed that for brittle materials, a pulverised material layer beneath the scratched grooves may appear as plastic deformation, forming ploughing ridges. After further investigating the materials in this pulverised region, Zhang concluded that the pulverised structure were actually micro crack clusters, which are easily removed by chemical etching. Visible cracks may appear beyond the pulverised region, as illustrated in figure 1. When scratch depth is less 1 μm, pulverisation appears even when almost no material is removed.

Molecular dynamics (MD) is an effective method of simulating the movement and interaction of molecules and atoms. It has been used to investigate the deformation mechanism during indentation and scratching on SiC. MD simulations primarily address the following research issues: subsurface deformation mechanisms, chip shape, and diamond tool wear. Most of the MD research regarding SiC focuses on 3C-SiC [12–15], while research on 4H-SiC and 6H-SiC remains relatively scarce. Moreover, some MD simulation studies set the system in two dimensions in order to reduce the amount of model calculation, thereby increasing the machinable distance and tool size in the simulations. Unfortunately, the reliability of the simulations may suffer as a result.

Wu *et al* [16] simulated the nano-cutting of 6H-SiC and confirmed that 6H-SiC undergoes amorphous structural transformation. Meanwhile, dislocations occurred in the subsurface and their propagation lead to a basal plane stacking fault. Nano-indentation results of high-resolution transmission electron microscopy confirm two major material deformation mechanisms, including amorphous deformation generation near the indentation region and dislocation propagation along both the basal and prismatic planes [17]. Different polytypes of SiC show different machining properties. As shown in figure 2, Luo *et al* [18] compared the nano-cutting of 3C-SiC, 4H-SiC and 6H-SiC. They found 4H-SiC exhibited superior subsurface integrity after machining, while 6H-SiC showed poorer results under a cutting depth of 1.3 nm. No dislocations were found in subsurface.

Considering the anisotropy of SiC, different crystal planes and orientations significantly influence the deformation mechanism and removal efficiency of the material. Meng *et al* [19] compared different combinations of crystal planes and orientations and found that machining on the surface of (01–10) with a cutting direction of [2-1-10] yielded a high removal rate and low abrasive wear for 6H-SiC, while the basal plane and the c-axis were difficult to machine. In addition to simulating traditional processing methods, MD has also been used to simulate femtosecond laser aided machining on 6H-SiC [20]. It was found that the modified 6H-SiC surface structure improved the removal efficiency and effectively reduced the depth of surface damage.

Single crystal 4H-SiC and 6H-SiC have obvious anisotropy, and the Si face and C face show different physical and chemical properties [21–23]. Both the C and Si faces can be used for epitaxial growth, but the Si face is the primary substrate candidate in commercial production due to the fact that its crystal lattice is better suited to epitaxial layer matching applications. Therefore, of the majority of reported research focus on the Si face [24–26], while studies the C face and comparisons between different face performances are limited [27]. Tian *et al* [28] compared the indentation of C and Si faces of 4H- and 6H-SiC through MD simulations and experiments. They found that the C face is more prone to dislocation on the basal plane than the Si face. Chen *et al* [29] found the Si face of 6H-SiC exhibited a higher material removal rate (MRR) than that of the C face during both mechanical polishing (MP) and chemical mechanical polishing (CMP) in an alkaline solution. The Si face may have removed more easily because it was oxidized by the dissolved oxygen. However, some researches show opposing results. Lu *et al* [30, 31] reported that the Si face is more difficult to remove than the C face during MP on both 4H- and 6H-SiC and considered that the variation in the MRRs was determined by the mechanical properties of different faces. Pan *et al* also reported that the C face of 6H-SiC showed higher MRR than the Si face in both acidic and alkaline solutions [32]. Therefore, differences between the MRRs of the Si face and C face are controversial. A fundamental understanding of the removal mechanism of

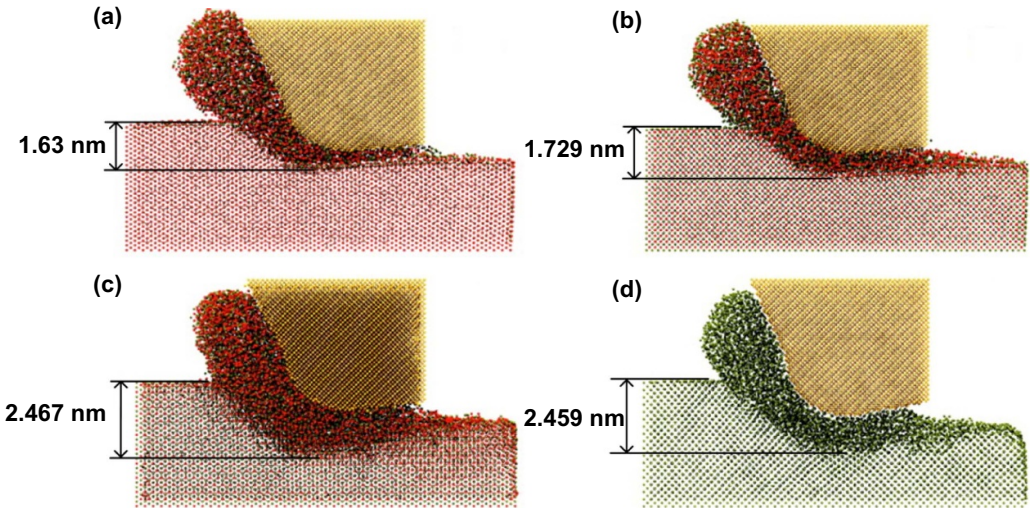

Figure 2. Subsurface deformation of Silicon Carbide and Silicon. (a) 4H-SiC, (b) 3C-SiC, (c) 6H-SiC and (d) Si [18].

4H-SiC and 6H-SiC is critical to provide a guide for improving polishing efficiency and quality.

This paper presents a study on the removal mechanism of 4H-SiC and 6H-SiC substrates during scratching using MD simulations in order to explain the differences in the machinability of the Si face and C face. Additionally, the quantified MD simulation results could provide a theoretical foundation that guides actual polishing of SiC.

2. Process model set up and MD analysis for SiC scratching simulation

For more than 250 polytypes of SiC, the crystal structures differ in the stacking sequence of the closed-packed layers. The stacking sequences of 4H-SiC and 6H-SiC are given by ABCB' and ABCA'C'B', respectively [1, 18]. Here, A, B, and C indicate the three possible lateral positions of the Si-C bilayers. A and A' bilayers have equivalent spatial positions, but their bonds are rotated 180 degrees with respect to each other. The molecule crystal structures of 4H-SiC and 6H-SiC are illustrated in figures 3(a) and (b). For both 4 H-SiC and 6 H-SiC, if the top surface is the Si face, the bottom surface will be the C face. In MD simulations, the Si atoms and C atoms are defined and distinguished by their different mass. Depending on the interest, the SiC workpiece can be positioned to align its C face or Si face to the cutting path plane.

The sample material block model for the MD simulation used in this study is shown in figure 3(c). The size of 4H-SiC or 6H-SiC workpiece was 40 nm × 19.7 nm × 12 nm ($x \times y \times z$), containing about 0.923 million atoms. The cutting tip of the abrasive grit was a hollow hemisphere on a cylindrical column with a of radius 5 nm to reduce the computation time. The abrasive cutting tip was positioned below the workpiece surface at the required cutting depth. The periodic boundary condition was applied in the y-direction while the fixed boundary condition was applied in the x- and z-directions.

The workpiece was divided into three layers: the Newtonian atoms (NVE ensemble), the thermostatic atomic layer (NVT ensemble) and the boundary atomic layer. The Newtonian atoms are the main part of the workpiece, following Newton's laws of motion, which are used to investigate the phenomena that occur during the scratching simulation [33–35]. The boundary atomic layer can prevent rigid movements of the entire workpiece during scratching. The thermostatic atomic layer can control the temperature within a specified range by adjusting the atomic velocity using a Berendsen thermostat. During scratching, the thermostatic atoms within the thermostatic layer absorbed the heat generated by the Newtonian atoms. In addition, the tip atoms were set as rigid bodies because the diamond tip is much harder than both 4H-SiC and 6H-SiC.

The selection of potential function for the MD analysis is critical to ensure the accuracy and reliability of the MD simulation. Appropriate potential functions can correctly simulate the behaviour of atoms to obtain accurate results [36, 37]. The Tersoff potential function is a three-body potential function that provides a more realistic description of covalently bonded materials [38]. Therefore, in this research, the Tersoff potential function is used to describe the interaction between C–C, Si–Si, and Si–C atoms as follows:

$$\mathrm{E} = \sum_i E_i = \frac{1}{2} \sum_{i \neq j} \mathrm{V}_{ij} \tag{1}$$

$$\mathrm{V}_{ij} = f_C(r_{ij}) \left[f_R(r_{ij}) + \mathrm{b}_{ij} f_A(r_{ij}) \right] \tag{2}$$

$$f_C(r) = \begin{cases} 1, & r_{ij} < R_{ij} \\ \frac{1}{2} + \frac{1}{2} \cos\left[\pi \frac{r_{ij} - R_{ij}}{S_{ij} - R_{ij}} \right], & R_{ij} < r_{ij} < S_{ij} \\ 0, & r_{ij} > S_{ij} \end{cases} \tag{3}$$

$$f_R(r_{ij}) = A_{ij} \exp(-\lambda_{ij} r_{ij}) \tag{4}$$

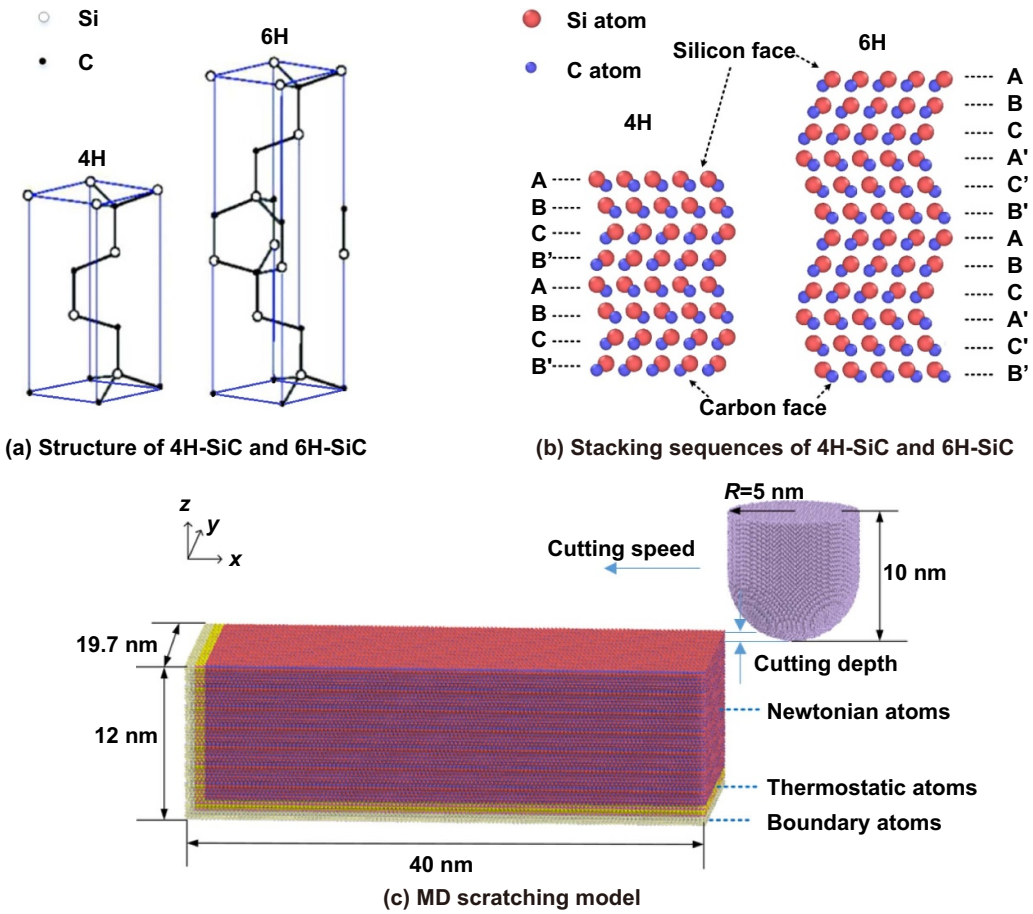

Figure 3. Silicon Carbide molecule models for MD analysis.

$$f_A(r_{ij}) = -B_{ij}\exp(-\mu_{ij}r_{ij}) \tag{5}$$

$$b_{ij} = \chi_{ij}\left(1+\beta_i^{n}\zeta_{ij}^{n}\right)^{-\frac{1}{2n}} \tag{6}$$

$$\zeta_{ij} = \sum_{k\neq i,j} f_C(r_{ik})\,\omega_{ij}\,g(\theta_{ijk}) \tag{7}$$

$$g(\theta) = 1+\frac{c_i^{2}}{d_i^{2}} - \frac{c_i^{2}}{d_i^{2}+(h_i-\cos\theta_{ijk})^{2}} \tag{8}$$

where E is the total energy; the sub-function, V_{ij}, describes the energy between two atoms (i and j); (i, j and k) label the three atoms of the system; f_{R} represents a repulsive pair potential; f_{A} represents an attractive pair potential; f_{C} represents a smooth cut-off function to limit the range of the potential; r_{ij} is the length of the i-j bond; b_{ij} is the bond order term; ζ_{ij} counts the number of other bonds to the i atom, besides the i-j bond; ω_{ij} is a constant set as 1 in this case [38]; θ_{ijk} is the bond angle between the i-j bond and i–k bond; and χ_{ij} is the mixing parameter depends on the different atom pairs. The parameters in Tersoff potential applied in this research are shown in table 1.

Table 1. Parameters in Tersoff potential for Si and C [38].

Parameters	Si–Si	C–C
A (eV)	1830.8	1393.6
B (eV)	471.18	346.7
λ (nm^{-1})	24.799	34.879
μ (nm^{-1})	17.322	22.119
β	1.1000×10^{-6}	1.5724×10^{-7}
n	0.78734	0.72751
c	1.0039×10^{5}	3.8049×10^{4}
d	16.217	4.3484
h	−0.59825	−0.57078
R (nm)	0.27	0.18
S (nm)	0.3	0.21
$\chi_{\mathrm{Si\text{–}Si}}=1.0$	$\chi_{\mathrm{C\text{–}C}}=1.0$	$\chi_{\mathrm{Si\text{–}C}}=0.9776$

The scratching processes were conducted on the (0001) basal plane (perpendicular to z-axis) along direction [1–210] (on the x-axis). The depth of scratching ranged from 0.5 nm to 3 nm, and the scratching speed was held constant at 100 m s^{-1}. The temperature of the thermostatic layer was controlled at 300 K during the simulation, and the relaxation process of the system was taken for 150 ps before the simulated scratching began. The simulation time step was set at 1 fs, and the

total scratching distance was set as 30 nm. The MD simulations presented in this paper were conducted and analysed using a large-scale atomic/molecular massively parallel simulator (LAMMPS) [39]. The MD results were visualized using OVITO [40] and the dislocation extraction algorithm (DXA) was used to analyse the deformation and dislocations that occurred during scratching [41].

3. Verification of MD simulation

The verification of MD simulation has always been a key challenge regarding its accuracy and reliability. The MD model used in this paper was experimentally verified by indentation and scratching tests previously reported in the literature [28]. The trends of the simulation and experimental results are consistent with those reported in other MD simulated indentation and scratching experiments on 4H-SiC and 6H-SiC. Therefore, the MD model provided a reliable trend projection. Further in this paper, the MD model is also verified in terms of forces and material removal rates.

Due to the limitation of scratching scales in experiments and MD simulations, it is difficult and unreliable to compare the results directly. Therefore, a specific force defined as force/scratching depth is adopted to compare the results from the MD simulations and scratching experiments, as shown in figure 4. For MD simulations in this research, the scratching depth is set as a constant of different values (e.g. 0.5 nm, 1 nm, 2 nm, and 3 nm), and the average tangential and normal forces on the scratching tip taken from the stable scratching stages are at the micron-Newton level. For the scratching experiments presented in reference [28], the scratching load was set as a constant (4 mN), and the average gouge depth obtained from the stable scratching stages was approximately 50 nm, which is much larger than the gouge depth presented in the MD simulation results in figures 4(a) and (b). The specific force provides a common platform for the comparison of the results from simulations and experiments.

Interestingly, in figure (a) and (b), the simulation revealed the following results for each cut depths between 0.5 and 3 nm: (1) the highest specific force value was recorded on the Si face of 4H-SiC, followed by the C face of 4H-SiC and the Si face of 6H-SiC; (2) the C face of 6H-SiC had the lowest specific force value. The experimental results in figure 4(c) show the same trend. Thus, it can be concluded that the specific scratching force on the C faces are lower than that on the Si faces, and the specific forces on 4H-SiC are greater than those on 6H-SiC. Even though the values of the ratios are significantly different due to the differences in tip sizes (5 nm in MD simulations and 3 μm in experiments) and scratching size scales, this trend is consistent with the experimental results in reference [28]. The specific forces decrease with the increase of scratching depth of cut as shown in figures 4(a) and (b). This phenomenon, known as the size-effect, commonly occurs in abrasive machining processes [42, 43].

Owning to current computing capacity, most MD simulations only analyse nanoscale mechanisms and phenomena and rarely extend to the actual machining scale. Additionally, the potential functions used in MD analysis only partially represent material performance under particular space scale and environmental conditions. Even so, MD analysis could provide sufficient information of material behaviours that match the tendency illustrated in experiments.

MRR is an important measure for evaluating the efficiency of various machining processes. Material removal is an important measure to assess the scratching efficiency of MD simulation analysis. Atom displacement—which refers to the atoms that move above the workpiece surface after the scratching tip passes—is often used to represent scratching performance. However, the grit-workpiece interaction area in figure 5(a) shows ridges of bulged atoms that form on either side of the scratching path as a result of the 'ploughing' action. These bulged atoms do not leave the workpiece, so they should not be included with the removed material. Only those atoms whose positions are higher than the ploughing ridge height can be defined as potentially removed atoms. Figures 5(b) and (c) provide the number of removed and displaced atoms from various scratching tests. It can be seen that the number of atoms above the original workpiece surface is significantly greater than the number of potentially removed atoms.

For the results of cut depths ranging from 0.5 to 3 nm, the C face shows more atom removal than the Si face. In the experimental results of reference [30], the MRR on the C face of 6H-SiC reached 13.94 nm min^{-1}, which was twice that the MRR observed on the Si face (6.13 nm min^{-1}). Although the simulated and experimental material removal performances were not directly comparable due to differences in scale, both results suggest that the C face exhibits significantly higher material removal efficiency than the Si face.

4. SiC deformation in the scratching processes

In MD simulation, the common neighbour analysis (CNA) and dislocation extraction algorithm (DXA) in Ovito are used to identify whether the lattice structure of a material is changed or damaged.

The CNA is an algorithm that computes a fingerprint of atom pairs to characterize the local structural environment [44]. The threshold distance criterion in CNA differentiates between bonded and unbonded pairs of atoms, which helps distinguish disordered atoms from perfectly structured atoms. For diamond structure, the algorithm analyses the local environment of each atom up to the second neighbour shell to determine the local structural type [45]. Here, the disordered atoms recognized by CNA are considered as atoms with amorphous structures.

The fundamental concept underlying the DXA is the Burgers circuit construction, which is the established method of discerning dislocations from other crystal defects and determining their Burgers vectors. In the formulation employed here, a Burgers circuit C is a path in the dislocated crystal consisting of a sequence of atom-to-atom steps (line elements Δx) [41]. There exists a mapping $\Delta x \rightarrow \Delta x$' that translates each line element of the path to a corresponding image, Δx', in a perfect

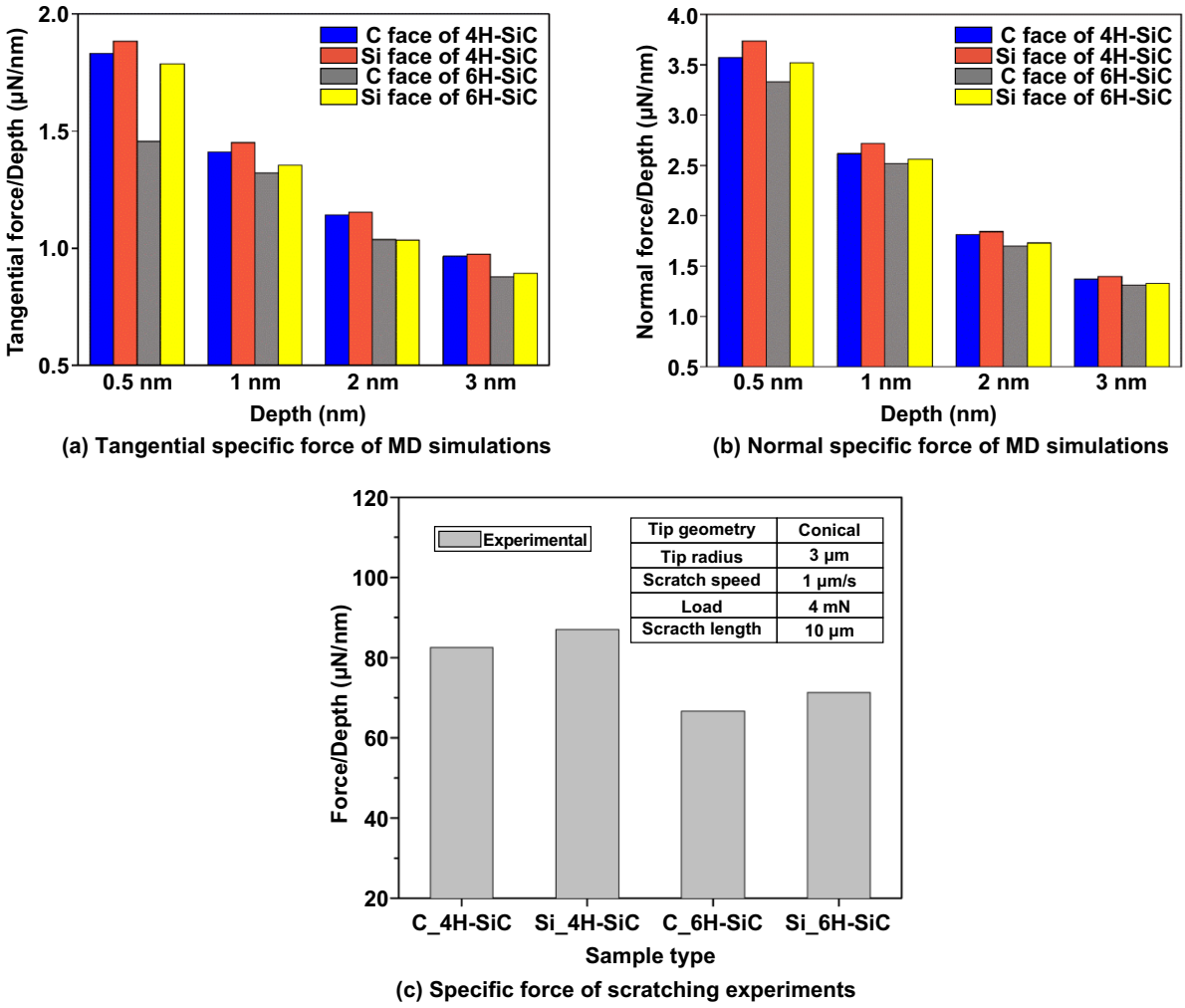

Figure 4. Comparison of specific scratching forces in MD simulations and experiments.

crystal lattice. As shown in figure 6, summing these transformed line elements algebraically along the associated path, *C*', gives the true Burgers vector of the dislocation enclosed by *C* [41]:

$$\mathrm{b} = -\sum_{C'} \Delta x. \tag{9}$$

Ductile-regime machining at the nanoscale can be achieved by the combination of dislocation activities and structural transformation [10]. This structural transformation can be considered as non-crystallization. Figures 7–9 show sectional views of the MD simulations. The white dots represent atoms with amorphous structures, while the blue and orange dots indicate atoms with a standard lattice structure, representing cubic diamond structures and hexagonal diamond structures, respectively. DXA also can identify dislocations, calculate the Burgers vectors and then display them as dislocation lines in Ovito [40].

4.1. Amorphisation

6H-SiC primarily underwent an amorphous transformation that could be considered plastic deformation [16]. Amorphous atoms are disordered atoms that have lost their regular lattice crystal structures as a result of scratching. Therefore, the amorphous atoms are considered as subsurface defects, which affect the properties of the material. All four structure cases had similar maximum depths of subsurface amorphous deformation. For both the 4H-SiC and 6H-SiC samples, the subsurface amorphous layers of C faces were relatively flat, while the Si faces developed uneven layers.

Undoubtedly, the amount of chips that accumulate in front of the scratching tip and subsurface damages increase as the scratch depth increases. When the scratch depth is small, the subsurface damage layer is shallow and relatively flat. When the scratch depth increases, the subsurface damage layer becomes thicker and uneven. It is interesting to note that the thicknesses of the amorphous deformations on the C face are less than those on the Si face. For example, at a scratch depth of 0.5 nm (figure 7), the maximum thickness of the amorphous deformation on the C face of 6H-SiC is only 0.87 nm, while

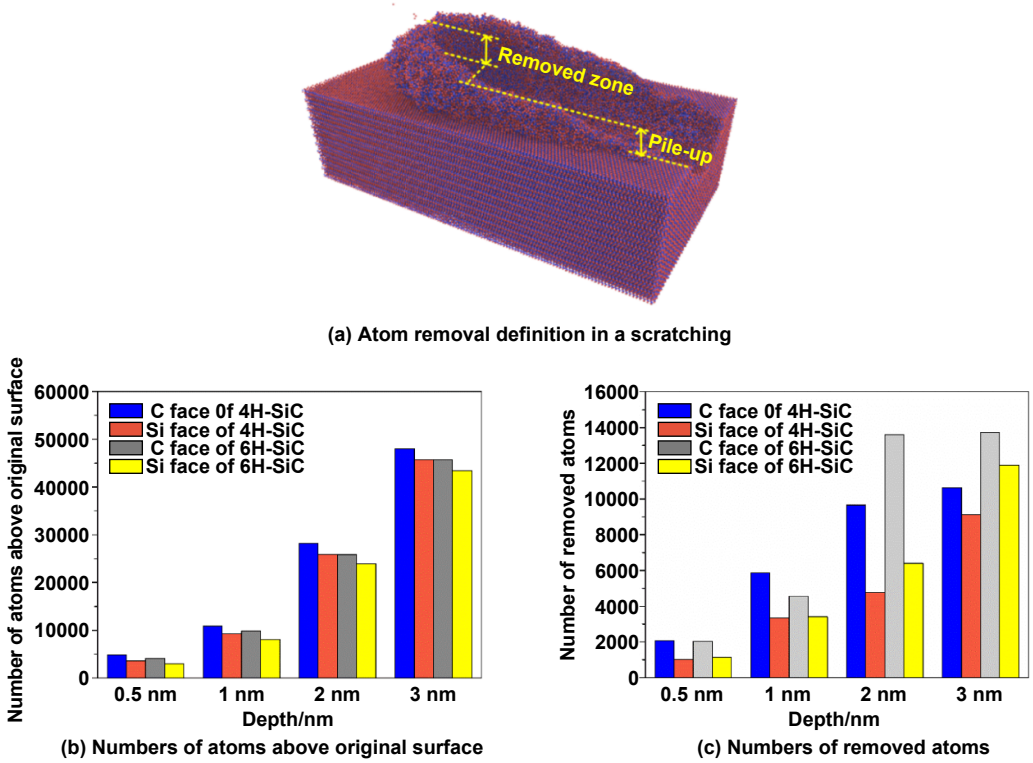

Figure 5. Cutting and ploughing actions in a scratching process.

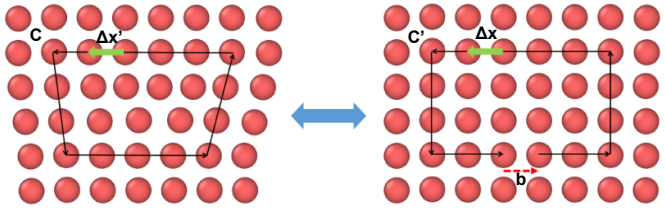

Figure 6. Schematic diagram of Burgers vectors.

that of the Si face reaches 1.73 nm. 6H-SiC shows thicker amorphous deformation than 4H-SiC at scratching depths over 2 nm.

The number of amorphous atoms in four cases was counted, as shown in figure 10(a). Interestingly, the C face shows fewer amorphous atoms than the Si face for both 4H-SiC and 6H-SiC. This means that the C face has less subsurface amorphous deformation and superior subsurface quality than the Si face at the same machining conditions, which is consistent with Lu's experimental conclusion [30].

4.2. Dislocation

In addition to amorphous atoms, aforementioned DXA can also identify atom dislocations that are a type of material deformation. In the analysis of DXA, atom dislocations refer to those atom movements with regular lattice structures [41]. In the DXA results, there were two main types of dislocations found in the subsurface of both 4H-SiC and 6H-SiC, along 1/3 < 1-210 > and 1/3 < 1-100 >. Figure 10(b) shows the number of dislocations that occurred in the subsurface of all the investigated cases. No dislocations developed at a scratch depth of 0.5 nm. The greater the scratch depth, the greater the number of dislocations. In particular, the C face can have up to twice as many dislocations as the Si face.

Here, the scratching simulations on the C and Si faces of 6H-SiC were selected as the example to investigate dislocation formation. Figure 11(a) shows the subsurface morphology of deformation using DXA. It can be seen that dislocations mainly occur on the (0001) basal plane and the (10–10) plane. The dislocations obtained in the MD simulation of Wu [16] principally occur on the (0001) and (11–22) planes. This difference may result from the MD model setup. Wu [16] applied 2.58 nm scratches in the y-direction, which is too thin to detect dislocations on the planes perpendicular to the *y*-axis. The Von Mises stress distribution of 6H-SiC during scratching is shown in figure 12. It can be seen that the stress concentration area is mainly located on the (0001) plane and (10–10) plane under the diamond tip. Dislocations are normally considered to be caused by the stress concentration during the scratching process, so stress distributions of the C face and Si face were analysed. Figures 13(a) and (b) show the changes of Von Mises stress in the local area before and after the dislocations occurred on the C face and Si face. The stress peaks shown in the figures may represent the occurrence of the dislocations. The stress peaks of dislocations on the C face (3148 MPa for the (0001) plane and 3972 MPa for the (10–10) plane) are lower than those on the Si face (3816 MPa for the (0001) plane and 4584 MPa for the (10–10) plane), which means that

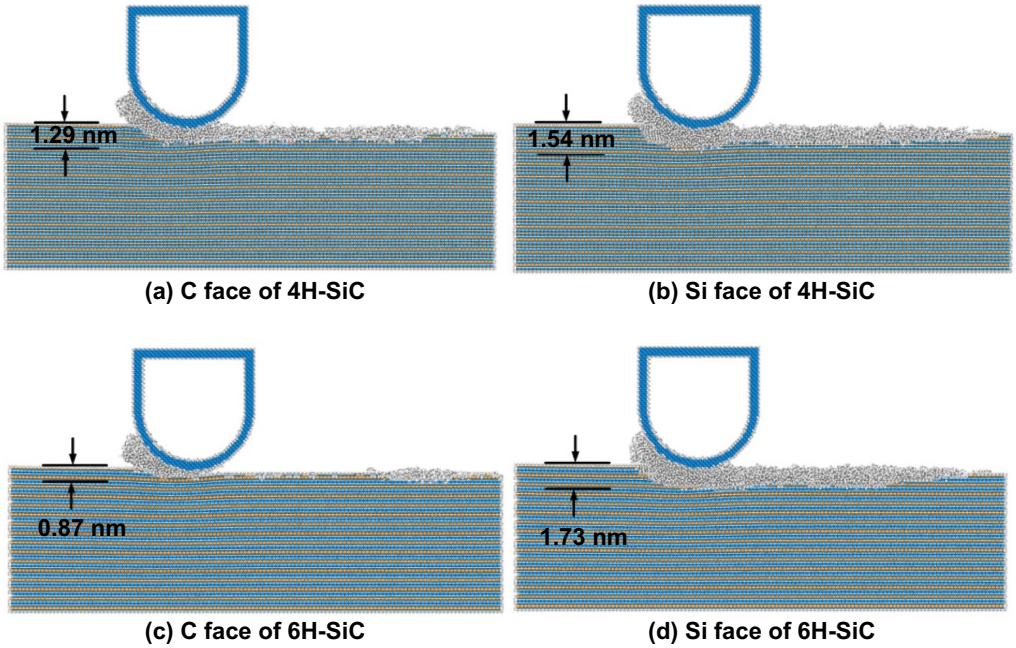

Figure 7. Sectional views of scratching at 0.5 nm obtained by DXA.

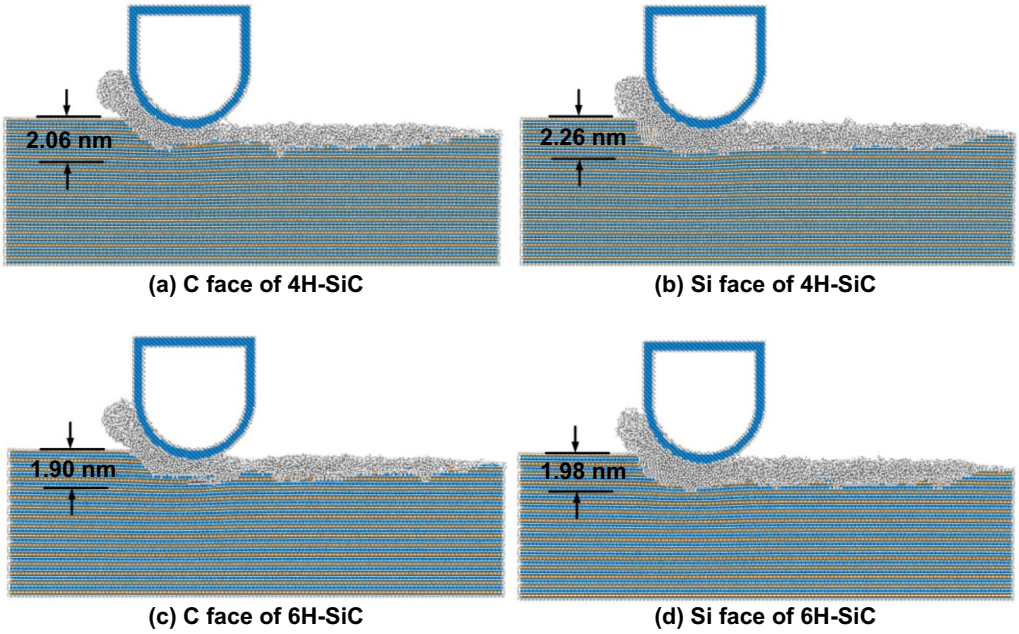

Figure 8. Sectional views of scratching at 1 nm obtained by DXA.

the C face is more prone to dislocations than the Si face under the same scratching conditions.

Considering the occurrence of dislocations on the C and Si faces, the critical stress of dislocations on the (10–10) plane is higher than that on the basal plane. The dislocations on the (10–10) plane of the C face occurred later than those on the basal plane, while dislocations on the basal plane occurred later on the Si face. All of these dislocations eventually led to slips along the scratching direction. Dislocations and slips on the basal plane may contribute to material removal and improve subsurface quality, while those on the (10–10) plane could cause severe subsurface layer cracks. This explains why the amorphous structures of the Si face are uneven and the amorphous structures of the C face are smoother as mentioned previously.

As shown in figure 14, a moving average with 30 data spans (equivalent to 0.3 nm) was applied to filter high-frequency noise from the force data of 6H-SiC at a scratching depth of 3 nm. The forces on the C face and Si face show similar fluctuation frequency ranging from 31.3 to 51.3 GHz (ΔL from

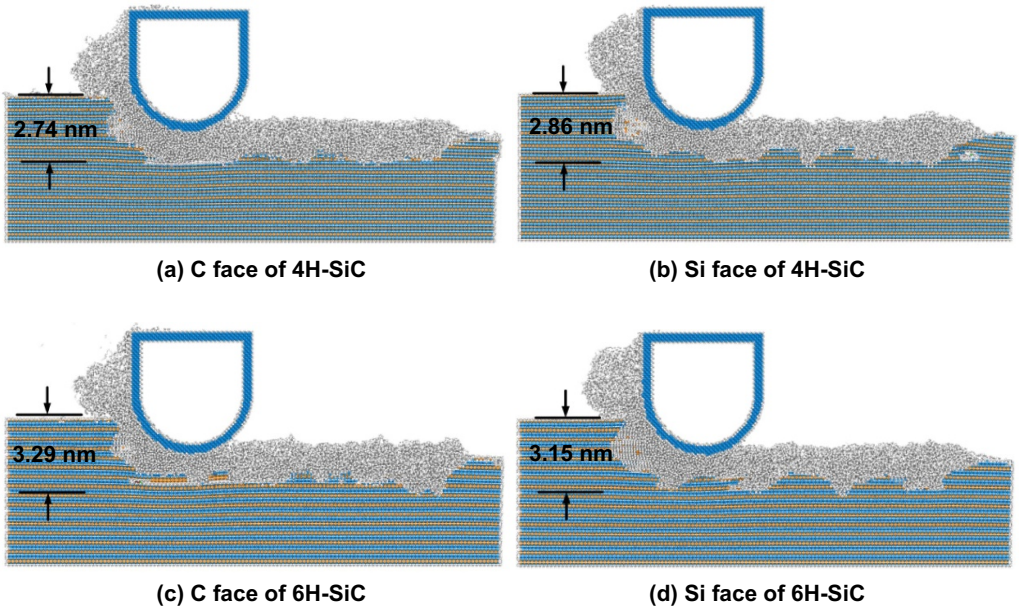

Figure 9. Sectional views of scratching at 3 nm obtained by DXA.

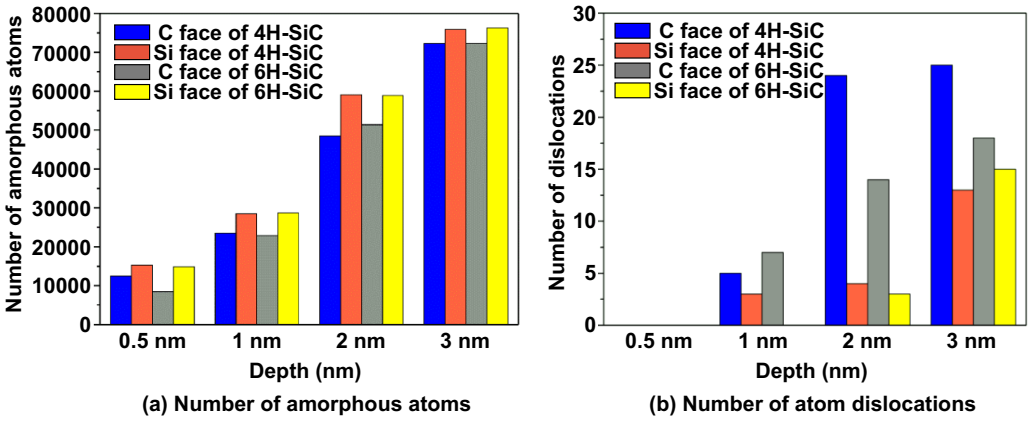

Figure 10. Numbers of amorphous atoms and dislocations in the subsurface of a scratching.

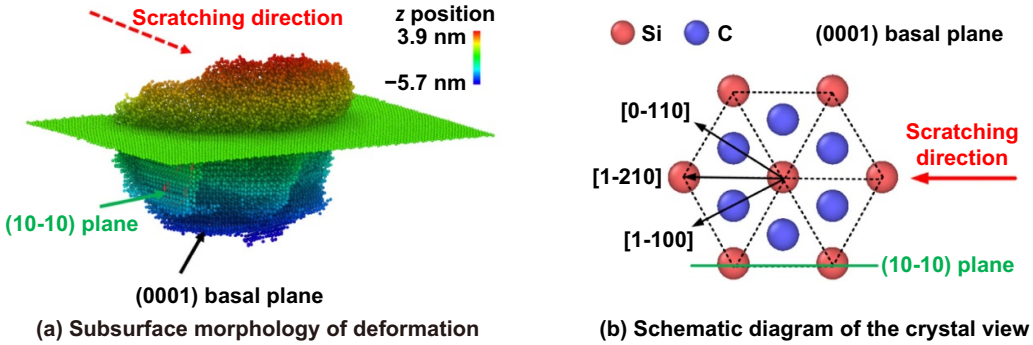

Figure 11. Deformation in the subsurface of a scratching and SiC basal plane view.

1.91 to 3.19 nm, and ΔT from 19.1 to 31.9 ps). In particular, the trends of both faces were almost identical before the stable scratching stage. The force of the Si face fluctuated while that of C face remained stable. Such a phenomenon may indicate that dislocations easily occur on the C face during scratching, which released stress fluctuation in the subsurface. In this way, the scratching force on the C face is lower and more stable than that on the Si face, and fewer amorphous atoms occurred in the subsurface, as shown in figure 10. A higher number of dislocations lead to a lower scratching force.

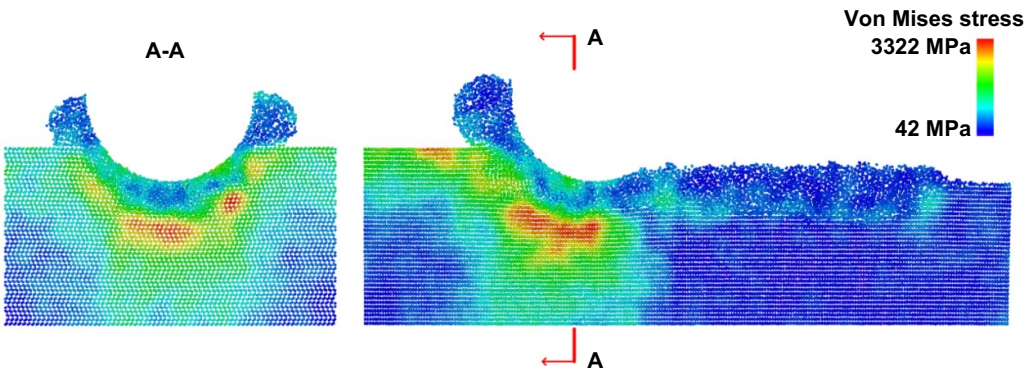

Figure 12. Von Mises stress distribution of 6H-SiC during scratching.

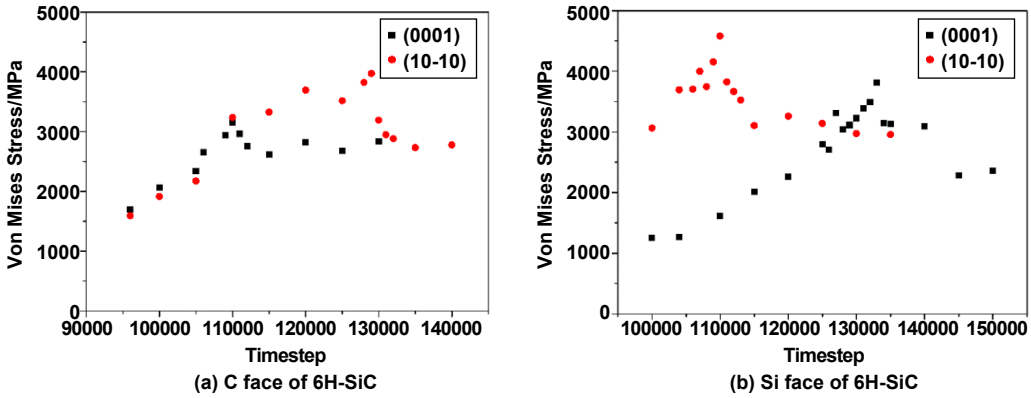

Figure 13. Von Mises stresses of in the scratching of 6H-SiC at different time steps.

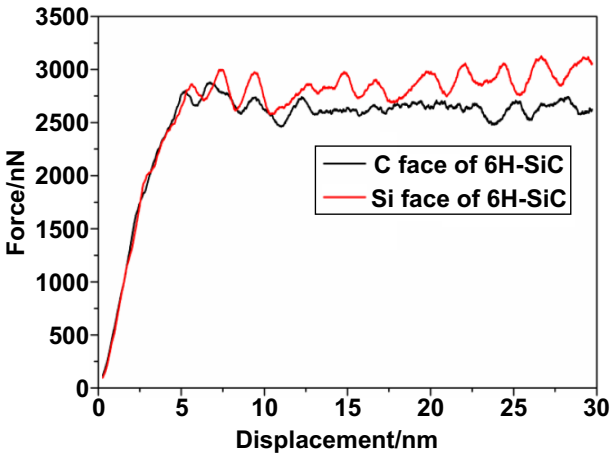

Figure 14. Forces of C face and Si face of 6H-SiC obtained by moving average at the scratching depth of 3 nm.

4.3. Materials removal and surface creation mechanism

For brittle materials, the subsurface damage generated after micro-scale processing was considered to be amorphous layer, pulverization layer and cracked [10, 11]. Brittleness and plasticity behaviours of the subsurface layer are controversial in nanoscale processing. As previously mentioned, dislocations do not occur unless the scratching depth exceeds the critical level. The initial contact between the scratch tip and the SiC sample also plays a crucial role in material removal. A previous investigation on nano-indentation [28] reported that amorphous atoms appeared in the subsurface layer, and dislocations and slippage occurred at a few nanometres level of engagement, as shown in figure 15. The hexagonal patterns are composed of two triangles facing opposite directions. The double triangular patterns on the Si face can reach depths of 6.0 and 6.2 nm below the original surface after indentation at a depth of 4 nm. However, this phenomenon was not obvious on the C face. The subsurface of the C face appears more like amorphous flake structures, which are related to the dislocations on the (0001) basal plane. Thus, the C face is more prone to dislocations and slippage on the (0001) basal plane, as analysed in section 4.2.

Figure 16 is a cross-sectional view of the 6H-SiC-scratched groove obtained by DXA. The amorphous atom region appears as an inverted triangle with distinct steps. These steps are six atom layers of atoms high, which is the height of the 6H-SiC unit cell. Dislocations on the (0001) basal plane were found under the right side of the groove. These results are highly consistent with the results from Meng's experiments [10], as shown in figure 17. Figure 17(b) also shows several dislocations on the basal plane in the subsurface of the scratch groove. As shown in figure 17(d), the amorphous layer region is also an inverted triangle, and a similar step shape can be seen on the

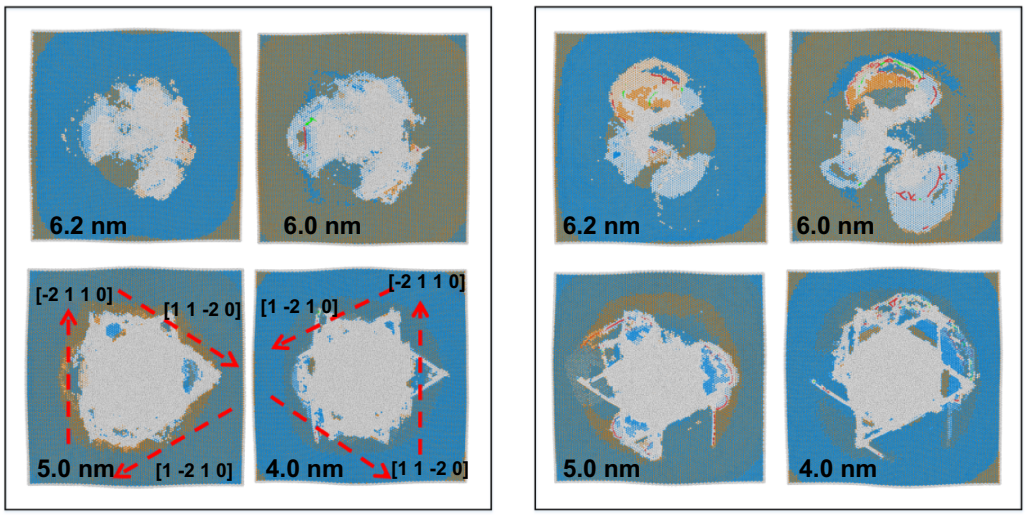

Figure 15. Horizontal sections of 6H-SiC at different depths after 4 nm indentation [28] (values in figure show the depth from the original surface).

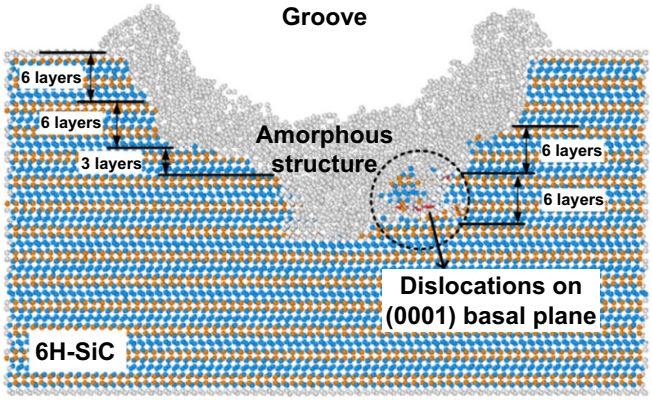

Figure 16. The cross-sectional subsurface image of 6H-SiC after scratching at the depth of 3 nm.

right side of the amorphous region. Thus, the step shapes that appeared in both the experiments and the simulations indicate that subsurface deformation gradually propagated downward during the scratching process. Additionally, the shape of groove is not symmetric in figure 16, because the SiC material shows anisotropy in its crystal structure. As shown in figure 3(b), the atomic arrangement of SiC is not symmetric, so the stress distribution (figure 12) and subsurface deformation are not symmetric under the same forces on both sides of the groove. This asymmetric feature can also be seen in experimental results as in figure 17(d). In particular, stacking faults and stress concentration are more likely to occur at the layer of those integer multiples of the 6H-SiC unit cell height.

Although there were no obvious cracks, irreversible dislocations occurred in the nanoscale scratching. Due to local temperature and stress changes during processing, these dislocations potentially form micro-cracks. In nanoscale machining, amorphous deformation is a plastic deformation, and atom dislocation is an elastic deformation initiated regular slip or split. Such a slip or split could promote micro-cracks formation at the nanometre level or plastic deformation if the bonds do not break. Some of the dislocations that occurred during scratching can recover after the tip passes the deformation area. The slip and micro-cracks generated by the dislocations on the base plane are beneficial to the removal of the material, while the dislocations on the (10–10) plane generated along the scratch direction may cause deeper and more serious structural damage. The atoms that accumulated in front of the cutting tip and at the ridges of cutting path were of disordered and amorphous structure, which appears to be plastic deformation.

5. Scratching performance in relation to SiC layer structure

4H-SiC and 6H-SiC are hexagonal diamond structures [46], stacked cyclically in the manner of ABCB' and ABCA'C'B', respectively—these patterns are also referred to layered structures. As analysed in section 4.2, the dislocations on the (0001) basal plane have positive contribution to material removal. Therefore, atom layer referenced scratching depths were selected in the simulations of 4H-SiC and 6H-SiC scratching processes to identify a potential beneficiary strategy for improving material removal efficiency. The scratching depths were set as an integral multiple of an atom layer in order to explore the beneficial behaviour of atom dislocation.

Figure 18 shows the atomic arrangement of the layer structures in 4H-SiC and 6H-SiC together with the thickness of the subsurface amorphous deformation at different scratching depths, which was set as integral multiples of an atom layer. There is no doubt that the subsurface amorphous deformation becomes more severe as more layers are removed. However, it is interesting to note that for 6H-SiC, there was only a slight increase in the thickness of the subsurface amorphous deformation when the scratching depth changed from layer

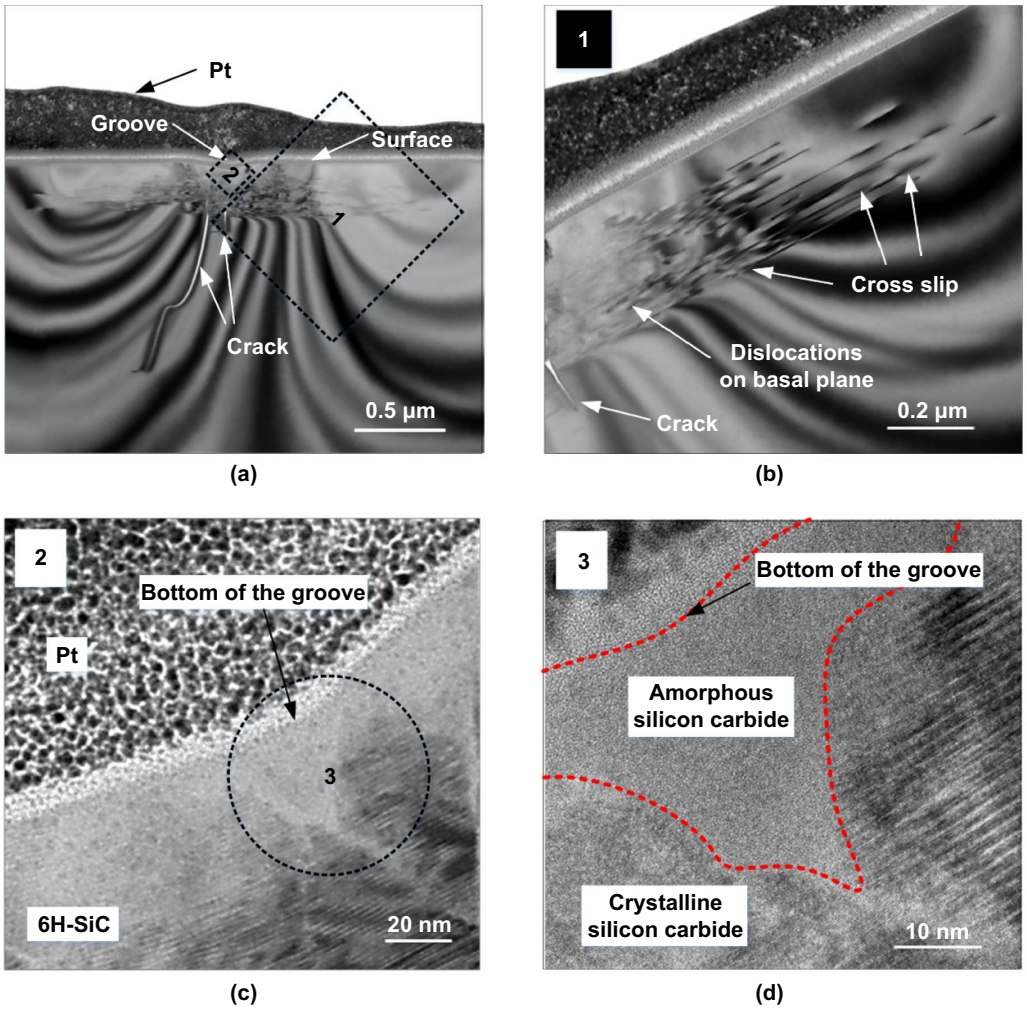

Figure 17. (a) Cross-sectional TEM image of 6H-SiC substrate after scratching test with 5 mN load by a tip with radius of 90 nm. (b) Magnified view of the regions indicated by circles 1 in a. (c) A bright-field TEM micrograph of the region at the bottom of the groove indicated by circles 2 in a. (d) A high-resolution TEM image of zone indicated by circle 3 in c. (after Meng, *et al* [10]).

three to layer four. Furthermore, when the scratching depth reached seven layers, the thickness of the subsurface amorphous deformation deceased. Figure 18(b) shows that the stacked structure of 6H-SiC between layers 6 and 7 flip their orientation from an arrow structure pointing left. Such a structural related plateau takes place every three layers. The fourth and seventh layers both correspond to the transition layer of 6H-SiC. Similarly, for 4H-SiC, the crystal structure flips every two layers. When the scratching depths are three and five layers, the thickness of the amorphous deformation increases less than at layers four and six. When the scratching depth for 4H-SiC reached seven layers, the thickness of the subsurface amorphous deformation slightly decreased.

The above observed phenomena indicate that the subsurface amorphous deformation does not increase proportionally with SiC molecule layers. Therefore, taking a scratching depth at the SiC atom orientation transition layer could be a beneficial choice for removing materials and obtaining superior substrate subsurface quality. Such a strategy might also be used to investigate the machining of other materials with layered structures.

In general, MD simulations can only be used to analyse atomic removal and deformation mechanisms qualitatively; it is difficult to provide quantitative guidance for actual machining because the potential function selected for the simulation may not accurately represent the molecular performance. Even so, the method proposed here is still a viable quantitative depiction of the actual process behaviour in relation to the material structure.

6. Remarks and conclusions

In general, MD simulations are commonly used to analyse atomic interactions and provide qualitative guidance for people to understand material removal mechanism at nanometre level. It is still a challenge to provide quantitative details because of the difficulties in acquiring a true molecular potential function that matches real application cases. Simulated and experimental results may conflict as a result of differences in scale. It is extremely difficult to conduct material mechanical removal experimentally at the molecular level.

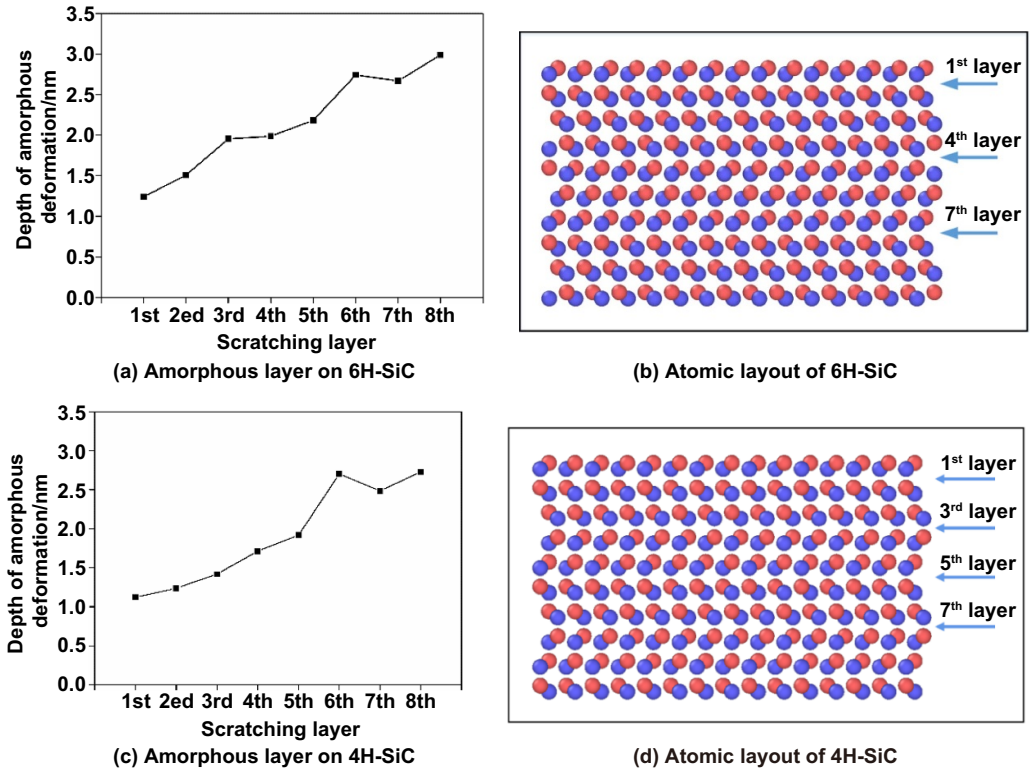

Figure 18. The thickness of the subsurface amorphous deformation at different scratching depths obtained by DXA.

By introducing a specific force as the ratio between cutting force and depth of cut, this paper provides a rational comparison between simulations and experiments. Although the material removal performance in the simulation presents similar trends, they do not match well quantitatively. This could be due to limited computing capacity which limits the scale of the MD simulations making it difficult to simulate the scratching process at the actual experimental size level. Continuous improvements in computing facilities will enhance the ability of simulations to match experiments in the near future. This paper provides insights into material removal mechanisms and potential guidance for polishing operation for improved machining surface quality. The methods introduced in this paper could also be applicable for the investigation of different SiC polytypes and other brittle materials.

The mechanisms of material removal and subsurface amorphous layer formation were observed and analysed through a series of scratching MD simulations on the C and Si faces of 4H-SiC and 6H-SiC. The following conclusions are drawn from the results:

- In nanoscale processing, material deformation in the forms of amorphous transformation and dislocations are the primary mechanisms of material removal, which are evidenced in both MD simulation and experiments. The failure of a brittle material, such as SiC, could appear as plastic deformation and brittle fracture. Both amorphous transformation and dislocation can present plastic deformations. However, the dislocations in the scratched 4H-SiC and 6H-SiC are prone to crack growth when the fractured bonds do not recover. Such dislocation-promoted fracture features can be seen in figures 15–17.
- During scratching, dislocations and slips occur on both the C face and the Si face, mainly on the (0001) basal plane and the (10–10) plane. Dislocations and slips on the (0001) plane promote material removal. Due to the lower stress fluctuation peak, dislocations at C face on the (0001) plane occur more readily.
- Material removal efficiency of the C face is higher than that of the Si face, and there is less subsurface amorphous deformation on the C face. Dislocations on the (0001) basal plane are more likely to occur on the C face than on the Si face, which leads to lower scratching forces, fewer amorphous atoms, and higher MRR on the C face.
- The MD simulation shows specific cutting forces decrease with the increase of cutting depth, which is consistent with the size-effect that is commonly observed in abrasive machining.
- MD simulation results show that setting the scratching cutting depth as an integer multiple of the height of a half lattice crystal may be more beneficial for removing materials and obtaining a substrate with better subsurface quality. This may guide and optimize the actual machining process. In addition, this analysis method may also be used to investigate the machining of other brittle materials with layered structures.

Acknowledgments

The authors acknowledge financial support from National Natural Science Foundation of China (Grant No.51835004 and 51575197), Huaqiao University International Cultivation Program for Outstanding Postgraduates and Subsidized Project for Postgraduates' Innovative Fund in Scientific Research of Huaqiao University (No. 18011080010). The Authors would like to express their gratitude to Feihu Zhang of Harbin Institute of Technology for allowing their results to be used in this research.

ORCID iDs

Zige Tian https://orcid.org/0000-0002-0869-7143
Xun Chen https://orcid.org/0000-0003-2547-9022

References

[1] Goel S 2014 The current understanding on the diamond machining of silicon carbide *J. Phys. D: Appl. Phys.* **47** 243001
[2] Perrone D 2007 Process and characterisation techniques on 4H-silicon carbide *PhD Thesis* Politecnico di Torino (https://www.researchgate.net/publication/238781248_Process_and_characterisation_techniques_on_4H_-_Silicon_Carbide)
[3] Lohrmann A, Johnson B C, McCallum J C and Castelletto S 2017 A review on single photon sources in silicon carbide *Rep. Prog. Phys.* **80** 034502
[4] Zhou Y, Pan G S, Shi X L, Gong H, Luo G H and Gu Z H 2014 Chemical mechanical planarization (CMP) of on-axis Si-face SiC wafer using catalyst nanoparticles in slurry *Surf. Coat. Technol.* **251** 48–55
[5] Demenet J L, Amer M, Tromas C, Eyidi D and Rabier J 2013 Dislocations in 4H- and 3C-SiC single crystals in the brittle regime *Phys. Status Solidi* c **10** 64–7
[6] Ravindra D and Patten J A 2011 Ductile regime material removal of silicon carbide (SiC) *Silicon Carbide: New Materials, Production Methods and Application* (New York: Nova) pp 141–67
[7] Goel S, Yan J W, Luo X C and Agrawal A 2014 Incipient plasticity in 4H-SiC during quasistatic nanoindentation *J. Mech. Behav. Biomed. Mater.* **34** 330–7
[8] Li Z P, Zhang F H and Luo X C 2018 Subsurface damages beneath fracture pits of reaction-bonded silicon carbide after ultra-precision grinding *Appl. Surf. Sci.* **448** 341–50
[9] Grim J R, Benamara M, Skowronski M, Everson W J and Heydemann V D 2006 Transmission electron microscopy analysis of mechanical polishing-related damage in silicon carbide wafers *Semicond. Sci. Technol.* **21** 1709
[10] Meng B B, Zhang Y and Zhang F H 2016 Material removal mechanism of 6H-SiC studied by nano-scratching with Berkovich indenter *Appl. Phys.* A **122** 247
[11] Zhang B and Tokura H 1988 Yoshikawa. Study on surface cracking of alumina scratched by single-point diamonds *J. Mater. Sci.* **23** 3214–24
[12] Noreyan A and Amar J G 2008 Molecular dynamics simulations of nanoscratching of 3C SiC *Wear* **265** 956–62
[13] Sun S, Peng X H, Xiang H G, Huang C, Yang B, Gao F S and Fu T 2017 Molecular dynamics simulation in single crystal 3C-SiC under nanoindentation: formation of prismatic loops *Ceram. Int.* **43** 16313–8
[14] Meng B B, Yuan D D and Xu S L 2019 Coupling effect on the removal mechanism and surface/subsurface characteristics of SiC during grinding process at the nanoscale *Ceram. Int.* **45** 2483–91
[15] Liu Y, Li B Z and Kong L F 2018 Molecular dynamics simulation of silicon carbide nanoscale material removal behaviour *Ceram. Int.* **44** 11910–3
[16] Wu Z H, Liu W D and Zhang L C 2017 Revealing the deformation mechanisms of 6H-silicon carbide under Nano-cutting *Comput. Mater. Sci.* **137** 282–8
[17] Wu Z H, Liu W D, Zhang L C and Lim S 2020 Amorphization and dislocation evolution mechanisms of single crystalline 6H-SiC *Acta Mater.* **182** 60–7
[18] Luo X C, Goel S and Reuben R L 2012 A quantitative assessment of nanometric machinability of major polytypes of single crystal silicon carbide *J. Eur. Ceram. Soc.* **32** 3423–34
[19] Meng B B, Yuan D D and Xu S L 2019 Atomic-scale characterization of slip deformation and nanometric machinability of single-crystal 6H-SiC *Nanoscale Res. Lett.* **14** 309
[20] Meng B B, Yuan D D, Zheng J and Xu S L 2019 Molecular dynamics study on femtosecond laser aided machining of monocrystalline silicon carbide *Mater. Sci. Semicond. Process.* **101** 1–9
[21] Kang C Y, Tang J, Li L M, Pan H B, Xu P S, Wei S Q, Chen X F and Xu X G 2012 In situ study on the electronic structure of graphene grown on 6H-SiCwith synchrotron radiation photoelectron spectroscopy *Appl. Surf. Sci.* **258** 2187–91
[22] Hu Y F, Zhang Y M, Guo H, Chong L Y and Zhang Y M 2016 Preparation of few-layer graphene on on-axis 4H-SiCsubstrates using a modified SiC-stacked method *Mater. Lett.* **164** 655–8
[23] Pan G S, Zhou Y, Luo G H, Shi X L, Zou C L and Gong H 2013 Chemical mechanical polishing (CMP) of on-axis Si-face 6H-SiC wafer for obtaining atomically flat defect-free surface *J. Mater. Sci., Mater. Electron.* **24** 5040–7
[24] Chen G M, Ni Z F, Xu L J, Li Q Z and Zhao Y W 2015 Performance of colloidal silica and ceria based slurries on CMP of Si-face 6H-SiC substrates *Appl. Surf. Sci.* **359** 664–8
[25] Kim H M, Oh J E and Kang T W 2001 Preparation of large area free-standing GaN substrates by HVPE using mechanical polishing liftoff method *Mater. Lett.* **47** 276–80
[26] Shi X L, Pan G S, Zhou Y, Gu Z H, Gong H and Zou C L 2014 Characterization of colloidal silica abrasives with different sizes and their chemical–mechanical polishing performance on 4H-SiC (0001) *Appl. Surf. Sci.* **307** 414–27
[27] Kubota A, Yoshimura M, Fukuyama S, Iwamoto C and Touge M 2012 Planarization of C-face 4H-SiC substrate using Fe particles and hydrogen peroxide solution *Precis. Eng.* **36** 137–40
[28] Tian Z G, Xu X P, Jiang F, Lu J, Luo Q F and Lin J M 2019 Study on nanomechanical properties of 4H-SiC and 6H-SiC by molecular dynamics simulations *Ceram. Int.* **45** 21998–2006
[29] Chen X F, Xu X G, Hu X B, Li J, Jiang S Z, Ning L N, Wang Y M and Jiang M H 2007 Anisotropy of chemical mechanical polishing in silicon carbide substrates *Mater. Sci. Eng.* B **142** 28–30
[30] Lu J, Luo Q F, Xu X P, Huang H and Jiang F 2019 Removal mechanism of 4H-and 6H-SiC substrates (0001 and) in mechanical planarization machining *Proc. Inst. Mech. Eng.* B **233** 69–76
[31] Luo Q 2018 *Research on Abrasive Polishing Removal Mechanisms of LED Substrates Materials* (Xiamen: Huaqiao University)

[32] Pan Z J, Feng B, Wang L and Hao J M 2013 Comparative chemical mechanical polishing studies of SiC (0001) and SiC (000-1) surface *Equip. Electron. Prod. Manuf.* **42** 19–23
[33] Goel S, Luo X C, Reuben R L and Rashid W B 2011 Atomistic aspects of ductile responses of cubic silicon carbide during nanometric cutting *Nanoscale Res. Lett.* **6** 589
[34] Zhang L C and Tanaka H 1999 On the mechanics and physics in the Nano-indentation of silicon monocrystals *JSME Int. J.* A **42** 546–59
[35] Goel S, Luo X C, Agrawal A and Reuben R L 2015 Diamond machining of silicon: a review of advances in molecular dynamics simulation *Int. J. Mach. Tools Manuf.* **88** 131–64
[36] Oluwajobi A and Chen X 2011 The effect of interatomic potentials on the molecular dynamics simulation of nanometric machining *Int. J. Autom. Comput.* **8** 326–32
[37] Oluwajobi A O and Chen X 2013 Effects of interatomic potentials on the determination of the minimum depth of cut in nanomachining *Int. J. Abras. Technol.* **6** 16–39
[38] Tersoff J 1989 Modeling solid-state chemistry: interatomic potentials for multicomponent systems *Phys. Rev.* B **39** 5566–8
[39] Plimpton S 1995 Fast parallel algorithms for short-range molecular dynamics *J. Comput. Phys.* **117** 1–19
[40] Stukowski A 2010 Visualization and analysis of atomistic simulation data with OVITO-the Open Visualization Tool *Modell. Simul. Mater. Sci. Eng.* **18** 015012
[41] Stukowski A, Bulatov V V and Arsenlis A 2012 Automated identification and indexing of dislocations in crystal interfaces *Modell. Simul. Mater. Sci. Eng.* **20** 085007
[42] Rowe W B and Chen X 1997 Characterization of the size effect in grinding and the sliced bread analogy *Int. J. Prod. Res.* **35** 887–99
[43] Heinzel C and Bleil N 2007 The use of the size effect in grinding for work-hardening *CIRP Ann.* **56** 327–30
[44] Honeycutt J D and Andersen H C 1987 Molecular dynamics study of melting and freezing of small Lennard-Jones clusters *J. Phys. Chem.* **91** 4950–63
[45] Maras E, Trushin O, Stukowski A, Ala-Nissila T and Jónsson H 2016 Global transition path search for dislocation formation in Ge on Si(001) *Comput. Phys. Commun.* **205** 13–21
[46] Yin L, Vancoille E Y J, Ramesh K and Huang H 2004 Surface characterization of 6H-SiC (0001) substrates in indentation and abrasive machining *Int. J. Mach. Tools Manuf.* **44** 607–15